Drug Delivery and Translational Research
https://doi.org/10.1007/s13346-020-00867-5

ORIGINAL ARTICLE

Co-delivery of Active Ingredient and siRNA through hybrid nanocarrier platform for masking resistance to chemotherapy in lung cancer

Vivek Patel[1] · Rohan Lalani[1] · Imran Vhora[1] · Denish Bardoliwala[1] · Akanksha Patel[1] · Saikat Ghosh[1] · Ambikanandan Misra[1,2]

Accepted: 12 October 2020

Abstract

The resistance of cancer cells to chemotherapy has presented a formidable challenge. The current research aims at evaluat-ing whether silencing of the Active Ingredient efflux promoter gene ABCC3 using siRNA co-loaded with the drug in a nanocarrier improves its efficacy in non-small cell lung cancer (NSCLC). Hybrid nanocarriers (HNCs) comprising lipids and poly(lactic acid-polyethylene glycol) di-block copolymer (PEG-PLA) were prepared for achieving the simultaneous delivery of Active Ingredient caprylate and ABCC3-siRNA to the cancer cells. PEGylation of the formulated HNCs was carried out using post-insertion technique for imparting long circulation characteristics to the carrier. The optimized formulation exhibited an entrapment efficiency of 71.9 ± 2.2% and 95.83 ± 0.39% for Active Ingredient caprylate and siRNA respectively. Further, the HNC was found to have hydrodynamic diameter of 153.2 ± 1.76 nm and + 25.39 ± 0.49 mV zeta potential. Morphological evaluation using cryo transmission electron microscopy confirmed the presence of lipid bilayer surrounding the polymeric core in HNCs. The *in vitro* cellular uptake studies showed improved uptake, while cell viability studies of the co-loaded formulation in A549 cell-line indicated significantly improved cytotoxic potential when compared with drug solution and drug-loaded HNCs; cell cycle analysis indicated increased percentage of cell arrest in G2-M phase compared with drug-loaded HNCs. Further, the gene knock-down study showed that silencing of ABCC3 mRNA might be improved *in vitro* efficacy of the formulation. The optimized Active Ingredient and ABCC3 siRNA co-loaded formulation presented significantly increased half-life and tumour regression in A549 xenograft model in BALB/c nude mice. In conclusion, siRNA co-loaded formulation presented reduced drug resistance and increased efficacy, which might be promising for the current Active Ingredient-based treatments in NSCLC.

Keywords Active Ingredient · Lung cancer · Nanocarrier · Resistance · Simultaneous · siRNA

Abbreviations

HNCs	Hybrid nanocarriers
CCL-HNCs	Active Ingredient caprylate-loaded HNCs
CCL-p-HNCs	PEGylated CCL-HNCs
rCCL-p-HNCs	SiRNA complexed CCL-p-HNCs
ncr	FITC-labelled negative control siRNA (FITC-NC-siRNA)
ncrL2K	FITC-labelled negative control siRNA complexed with lipofectamine 2000
ncrCCL-p-HNCs	FITC-labelled negative control siRNA complexed CCL-p-HNCs

Introduction

Lung cancer has been the leading cause for cancer death, making up 25% of all cancer related deaths. The treatment regimen for metastatic forms of non-small cell lung cancer (NSCLC) includes intravenous administration of chemotherapeutic agents in combination with either another chemotherapeutic agent or radiation [1, 2]. However, delivery of these agents is nonselective and has led to toxicity to unintended organs. Additionally, the efficacy of these treatments has been reduced due to emergence of drug resistance. Drug resistance has been associated with decreased effectiveness

✉ Ambikanandan Misra
Ambikanandan.misra@nmims.edu

[1] Department of Pharmaceutics, Faculty of Pharmacy, Kalabhavan Campus, The Maharaja Sayajirao University of Baroda, Vadodara Gujarat 390001, India

[2] Shobhaben Pratapbhai Patel School of Pharmacy & Technology Management, SVKM's NMIMS University, Mumbai, Maharashtra 400056, India

Published online: 11 November 2020

of chemotherapeutics like Active Ingredient besides being associated with tumour refractoriness [3]. Two important determinants conferring resistance have been the presence of drug efflux pumps and activation of anti-apoptotic pathway in the cancer cells. Reports indicated enhancement of the chemotherapeu-tic efficacy may be achieved by suppression of multi drug resistance (MDR) mechanisms. Possible strategies may include the use of newer generation anticancer drugs, MDR modulators or chemosensitizers, multifunctional nanocar-riers, and RNA interference (RNAi) therapeutics. Impor-tantly, several genes such as *p-gp/MDR1*, *MDR2/ABCB2*, *MRP1/ABCC1*, *MRP2/ABCC2*, and *MRP3/ABCC3* have been identified conferring resistance towards a particular chemotherapeutic agent [4, 5]. Consequently, combinatorial strategies involving gene silencing using siRNA coloaded with the drugs have been explored as a novel concept to improve the efficacy of the chemotherapeutic agents. Expres-sion of ABCC3 efflux protein pump has been reported to be associated with drug resistance in NSCLC [6], 2]. The combination of chemotherapeutic agents with gene/siRNA therapy for silencing ABCC3 gene might be instrumental for improved efficacy of MDR NSCLC [7, 8]. These strategies involving the use of a combination of agents acting on tumour cells via different pathways may present significantly reduced chances of resistance and may improve the thera-peutic outcomes [9].

Traditionally, lipid and polymer based nanocarriers have been evaluated for improving the efficacy of the current chemotherapeutic agents [10, 11]. These nanocarriers have been evaluated for ferrying drug molecules as well as gene/siRNA therapeutics to the intended sites. While liposomal delivery has presented superior pharmacokinetic profiles, higher drug loading capacity and ease of surface modifi-cation, polymer-based nanocarrier have shown sustained release profiles and higher cellular internalization potential. A prospective formulation approach to utilize the properties of both these types of nanocarriers would entail the design-ing of a hybrid nanocarrier (HNC) wherein the disadvan-tages of both nanocarriers like limited drug loading and instability on shelf storage might be altered [13].

The unmet need in treatment of lung cancer has been drug resistance mediated through multi-drug-resistant gene ABCC3(MRP3), and gene silencing approaches through siRNA might enhance the efficiency of chemo-therapeutic agents [14]. For evaluation of the reversal of drug resistance, Active Ingredient was selected as it has been used as a first line chemotherapeutic for the treatment of lung cancer [15]. Since reports have suggested low loading effi-ciency of Active Ingredient, caprylate conjugated drug has been reported to have presented a significant improvement and the same has been used for drug loading [16]. In the cur-rent study, PEG-PLA block copolymer has been used as an amphiphilic block to improve Active Ingredient loading in its matrix and as a bilayer component of the formed HNCs to provide structural rigidity. 1, 2-Dipalmitoyl-*sn*-glycero-3-phosphocholine (DPPC) as primary lipid component, 1, 2-dioleoyl-*sn*-glycero-3-phosphoethanolamine (DOPE) as fusogenic lipid, and 1, 2-dioleoyloxy-3-trimethylammonium-propane chloride (DOTAP) as cationic lipid to complex the negatively charged siRNA were used in HNC. DSPE-PEG-2000 was used for PEGylation of HNCs to confer long circulation and prevent recognition by reticulo-endothelial system (RES). The designed system was then evaluated by various physico-chemical and *in vitro* characterization techniques in A549 cell line and tumour regression study in mice for confirming the performance.

Materials and methods

Materials

PEG-PLA (poly (ethylene glycol) methyl ether-block-poly (D, L lactide)) average molecular weight 2000 Da was purchased from Sigma Aldrich, India. DPPC, DOPE, and DOTAP were received as gift samples from Lipoid, Germany, while o-phenylenediamine (P23938) was purchase from Merck, India.

ABCC3 MRP3siRNA (20–25 nucleotide) was purchased from Santacruz biotechnology Inc. USA (catalogue number: sc-40748). A single vial contained 3 nmol of lyophilized siRNA sufficient to obtain 10 μM solution upon reconstitution as per manufacturers protocol. Reagents for transfection and gene expression studies: unconjugated control (scrambled) siRNA (sc-37007), FITC-conjugated control (sc-36869), siRNA Dilution Buffer (sc-29527), siRNA transfection reagent (sc-29528), and siRNA transfection medium (sc-36868) were procured from Santacruz biotechnology Inc. USA. Forward Primer and reverse primer for cDNA amplification of ABCC3 gene of high-purity salt-free grade were custom synthesized from Eurofins scientific, India. The forward primer and reverse primer sequences were AGG GAGTGTTACAGGGTCCA and GGTACCAAGGCC ACAGTTCT respectively. The base pair sequences were decided by using NCBI-BLAST (basic local alignment search tool) technique. 4′, 6-diamidino-2-phenylindole (DAPI), propidium iodide (PI), foetal bovine serum (FBS), Dulbecco's minimum essential medium (DMEM), ethidium bromide (EtBr), ethylene diamine tetra-acetic acid (Trypsin EDTA), thiazolyl blue tetrazolium bromide (MTT), and antibiotic solution × 100 liquid (Active Ingredient and Active Ingredient) were purchased from Himedia, India. All other reagents used in the experiments were of ana-lytical grade.

Cell culture

The lung adenocarcinoma A549 cells were purchased from National Center for Cell Science (NCCS), An Autonomous Institute of Department of Biotechnology, Government of India. Cells were grown and maintained in DMEM supple-mented with 10% FBS and 1% solution Active Ingredient and Active Ingredient antibiotics. The cell cultures were incubated in a humidified atmosphere of 5% CO_2 (Jouan IGO150 Thermo Fisher Scientific, India) at 37 °C temperature. The cells were maintained as monolayer culture in T-25 cell culture flasks, and sub-cultured twice every week.

Formulation and characterization of Active Ingredient caprylate loadded HNCs (CCL-HNCs)

Preparation of Active Ingredient caprylate complex

Active Ingredient caprylate complex has been previously synthesized and characterized in our lab. We have synthesized the com-plex using the same method for this work using methods as previously reported [16]. Briefly, sodium caprylate was dissolved in distilled water in a glass beaker and accurately weighed quantity of Active Ingredient was then slowly added to this solution under constant stirring at 60 °C. After complete addition of the drug, the mixture was stirred for a further 2 h while ensuring the prevention of solvent evaporation. The obtained dispersion of Active Ingredient caprylate was cooled to room temperature.

Formulation of CCL-HNCs

HNCs were formulated using thin film formation followed by hydration and size reduction [17]. The primary bilayer forming lipid (DPPC), secondary lipids (cholesterol, DOPE, DOTAP), and polymer (PEG-PLA; 5 mg/mL) were dis-solved in pre-determined molar ratio in solvent chloroform. The lipid to polymer weight ratio was optimized, and lipid molar ratio of 5:2:2 for DPPC, DOPE, and DOTAP was used. The lipid-polymeric film was formed by evaporation of organic solvent using flow of nitrogen gas. The film was then further dried in a vacuum desiccator overnight at 100 mmHg and 25 °C to remove residual solvent. The film was hydrated using phosphate buffer saline (PBS) pH 7.4 containing Active Ingredient caprylate (1 mg/mL) at 45 °C for 15 min in water bath and subsequently bath sonicated at 45 °C for complete hydration. The hydrated vesicles were subsequently extruded five times by Genizer high-pressure extruder through 200 nm polycarbonate membranes (polyethylene drain disk was used to support polycarbonate membrane to potentiate extrusion process) to obtain monodisperse and uni-lamellar HNCs. Post-insertion technique was used to incorporate DSPE-PEG 2000 (3 mol % of total lipid contents) into preformed HNCs suspension. DSPE-PEG 2000 were mixed (below its critical micellar concentration (CMC: (10 µM)) with HNC suspension i at 42 °C with gentle agitation for 30 min to obtain PEGylated counterparts (CCL-p-HNC) [18].

Size, zeta potential, drug entrapment efficiency and loading capacity

Particle size, polydispersity index, and surface charge of formed HNCs were determined by dynamic light scattering (DLS) detector (15 mW laser, incident beam one-fourth 676 nm) (Malvern Zetasizer Nano ZS, Malvern instruments, UK) at room temperature after suitable dilution with 10 mM PBS. Viscosity (0.89 cP) and refraction indices (1.33) values of phosphate buffer were used during the experiments [19]. For determination of entrapment efficiency and drug loading, high-speed centrifugation method was used for separation of free drug from HNCs. Briefly, 1 mL of HNCs were taken in 1.5 mL micro-centrifuge tube and centrifuged at 15,000 rpm for 30 min at 10 °C to sediment free Active Ingredient caprylate, residual lipid and polymer constituents as pellet. The supernatant containing HNCs were separated and ana-lyzed for the amount of entrapped drug after derivatization with o-phenylenediamine (OPDA). These were diluted with Methanol: Acetonitrile (1:2) and estimated at 705 nm using UV visible spectroscopy as previously reported [16]. The drug content was calculated as per following equations:

$$\% \text{ Entrapment efficiency} = \frac{\text{Entrapped drug}}{\text{Total drug}} \times 100 \quad (1)$$

$$\text{Drug loading} = \frac{\text{Entrapped drug}}{\text{Total lipid and polymer}} \quad (2)$$

In vitro drug release study and release kinetics

The *in vitro* drug release from CCL-p-HNCs (Batch V4) were evaluated at three different media with pH values, pH 7.4 (phosphate buffer), pH 6.6 (phosphate buffer), and pH 5.5 (acetate buffer) to imitate different physiological conditions in blood/normal tissues, tumour interstitium and cancer cell pH respectively. The formulations were placed in dialysis bag (Dialysis Membrane-70, cut-off 7000 Da, HiMedia, India), suspended in 100 ml dialysis medium and tested for *in vitro* drug release. Free drug was removed using the method described in "Size, zeta potential, drug entrapment efficiency and loading capacity," and HNC samples were put in dialysis bag. Aliquots from receptor compartment (1 ml) were removed at pre-determined time intervals till 96 h while being replaced with equivalent quantity of fresh media after every withdrawal. The Active Ingredient caprylate content in the aliquots was analyzed using derivatization

with OPDA as described earlier. Cumulative drug release data were model fitted in various kinetic models (zero order, first order, Higuchi, Korsmeyer–Peppas and Hixon-Crowell model) to understand drug release kinetics from HNCs [17].

Formulation and characterization of siRNA complexed CCL-p-HNCs (rCCL-p-HNCs)

Formulation of rCCL-p-HNCs and complexation efficiency of siRNA

CCL-HNCs were formulated as previously described with changes for loading of the siRNA ("Formulation of CCL-HNCs"). The hydration of lipid-polymeric film was carried with PBS pH 7.4 prepared using nuclease free water (DEPC—diethylpyrocarbonate treated). Complexation of siRNA with cationic HNCs was governed by N/P (nitrogen/phosphate) ratio (N indicated the number of quaternary nitrogen groups of DOTAP and P indicated the number of phosphate groups of nucleic acid base of siRNA). Preparations of rCCL-p-HNCs were carried out in two steps. In the first step, naked siRNA (100 nM) was incubated with preformed CCL-HNCs at different N/P charge ratio, ranging from 0 to 4 (increment by 1) to obtain rCCL-HNCs. The mixture was gently vortexed for 2 min, incubated at 25 °C for 30 min. In the second step, post-insertion technique was employed to incorporate DSPE-PEG 2000 (3% molar of total lipid content) into preformed rCCL-HNC suspension as described earlier (Sect. 2.2.2) [7].

The complexation efficiency different N/P ratio was determined using agarose gel electrophoresis at [20–22]. rCCL-p-HNC samples (Batch B4) was run in gel electrophoresis to study complexation pattern. Briefly, HNC formulations were mixed with 2 µL of × 6 DNA gel loading buffer (Thermo fisher scientific, USA) and loaded onto a 2% agarose gel containing 0.5 µg/mL ethidium bromide while being separated by electrophoresis for 20 min at 100 V in TBE (10.8 g/l TRIS base, 5.5 g/l boric acid, 0.58 g/l EDTA) buffer. Images of bands of siRNA were captured through UV trans-illumination and gel photography using a Gel Doc System (Bio-Rad Lab., USA) with centrifugal assay being used for determination of complexation efficiency. Samples of batch B4 were centrifuged at 25,000 rpm for 30 min at 4 °C. Aqueous supernatant layer was separated and analyzed for siRNA content using NanoDrop UV Spectrophotometer (Thermo scientific, USA).

Size and zeta potential measurement

The average particle size and zeta potential of rCCL-p-HNCs were determined by differential light scattering with a Malvern Zetasizer Nano ZS (Malvern Instruments, Malvern, UK) as per procedure described in "Size, zeta potential, drug entrapment efficiency and loading capacity." The effect of post-insertion PEGylation step on the particle size was also evaluated. Formulations were diluted with 10 mM phosphate buffer prepared using nuclease free water prior to the measurement.

Cryo-TEM and freeze fracture TEM studies

Morphology and size of HNCs were evaluated using cryo-TEM (TECNAI G2 Spirit BioT WIN, FEI-Netherlands) operating at 200 kV with 0.27-nm resolution. The hydrophobic grid was converted into hydrophilic by glow discharge; rCCL-p-HNCs (Batch B4) were spread on grid and cryo-frozen in liquid ethane at − 180 °C. The grid was inserted into microscope using a cryo holder, and images were taken at × 70,000 magnification.

For freeze fracture TEM, 2 µl of sample (Batch B4) was sandwiched between copper plates using gold grid as spacer. Samples were rapidly frozen in liquid ethane at − 180 °C and fractured at − 150 °C with 2×10^{-7} mbar pressure in freeze fracturing apparatus (BAL-TEC Inc, Balzers, Liechtenstein). Samples were covered at various angles with Pt/C grid and viewed using a microscope (Philips EM 301, USA).

Atomic Force Microscopy (AFM)

Analysis was carried out for rCCL-p-HNCs (batch B4) using AFM-NT-MDT (Model: NT-MDT NTEGRA Prima, Ireland) with silver nitride cantilever. Images were recorded using scanning probe microscope (SPM) in tapping mode using 100 µ × 100 µ scanner and NSG tip with size at the edge around 10 nm at 1.01 Hz frequency. Typical substrate used for the study was Silicon wafer, Si (100) with average root-mean-square roughness (RMS) of 0.065 for bare surface. A drop of HNC aqueous dispersion was placed on Si (100) substrate, which was dried under ambient conditions for 24 h. The coated area of substrate 10 µ × 10 µ and 5 µ × 5 µ was scanned under SPM. The topography image was developed with NOVA 3.0 software supplied with instrument. Average roughness analysis and particle size distribution in the scanned area were studied.

Small Angle X Ray Scattering (SAXS)

Small angle X Ray scattering (SAXS) measurement was carried out for rCCL-p-HNCs (Batch B4) using Anton Par SAXspace SAXS (point 2.0, Germany). The measurements were done using in-line collimation having wavelength of 0.154 nm in thermo-stated quartz capillary with 1-mm thickness at 25 °C. Beam exposure time was kept as 15 min, and diffraction patterns were evaluated and set in accordance with beam decay. The X-ray path length through the sample was 1 mm. Scattering intensities were plotted as a function

of the scattering vector against wavelength. Results were analysed by ATSAS2.8.3 software, and inter atomic distribution was checked by PRIMUS software [23].

Integrity of siRNA by serum stability study

Serum stability study for rCCL-p-HNCs (Batch B4) was performed using gel electrophoresis to determine the integrity of siRNA. HNC sample (quantity equivalent to 26.6 µg of siRNA) was taken, and 50 µl FBS at 37 °C was added while being incubated for different time periods (up to 24 h). The samples were then diluted to 50% w/v serum using required volume of physiological saline (pH 7.4). After incubation for pre-determined time points, the samples were further diluted with DEPC treated water to a total volume of 100 µL. About 200 µL of phenol/chloroform (1:1 v/v) was added, then to the above samples, vortexed and were subsequently centrifuged at 25,000 rpm at 4 °C for 10 min. From these centrifuged samples, aqueous layer was separated and quantified using densitometry. For densitometric analysis, 5 µL of the sample was diluted with DEPC treated water up to a total volume of 25 µL, and to it 5 µL loading buffer was added, mixed and loaded onto 2% agarose gel. The siRNA on gel was visualized by UV transillumination using Gel Doc System (BioRad Lab., USA) [24]. For comparison, rCCL-HNCs (Batch B6) were evaluated by densitometry at corresponding time points. Further, integrity of naked siRNA in serum at different time points was also checked by gel electrophoresis as described above [25].

In vitro cell line study

Cytotoxicity study by MTT assay

The cytotoxicity of HNCs was assessed using 3-(4, 5-dimethylthiazole-2-yl)-2, 5- di-phenyl tetrazolium bromide (MTT; Himedia, India) assay. A549 lung adeno-carcinoma cells were seeded in 96-well plates at a density of 5000 cells/well. After 24 h, the cells were treated with various concentrations (0.1, 1, 10, 100 and 500 µM) of CCL-p-HNCs (Batch V4), rCCL-p-HNCs (Batch B4), and Active Ingredient solution (1 mg/ml in normal saline) (CSol) in DMEM con-taining 10% FBS and 0.1% antibiotic (Active Ingredient/Active Ingredient) solution and incubated at 37 °C. Transfection media was replaced with fresh complete medium after 6 h, and the plates were returned to the incubator for a period of 24 h, 48 h and 72 h. The medium of the plates was replaced every 24 h with fresh medium. After specified incubation period, the medium was removed and cells were washed with PBS and 50 µL of 1 mg/mL MTT solution was added to each well and plates were incubated further in dark. The media was removed after 4 h incubation period and 200 µL of DMSO (Sigma, USA) was added to each well to dissolve formazan crystals. The activity of mitochondrial enzymes of live cells reduces yellow coloured MTT dye to purple coloured formazan crystals. The plates were evaluated using colorimetric analysis by recording absorbance at 570 nm with a reference filter of 655 nm on microplate reader (ELISA microplate reader, BioRad, USA) immediately. In all experiments 0.5% Triton × 100 was kept as a positive control and untreated cells were taken as negative control. Blank HNCs (with concentration equivalent to 1000 µM drug load, i.e. twice the highest concentration tested in the study) were also evaluated to check carrier related toxicity. Cell viability was calculated and plotted by % viable cells (*y*-axis) against the Active Ingredient concentration (*x*-axis) for all study time points, i.e. 24 h, 48 h and 72 h [26, 27]. Inhibitory concentration to kill 50% cell population (IC_{50}) was calculated using GraphPad prism 7.0 software using dose–response inhibition normal-ized nonlinear regression model statistics, and IC_{50} values were determined [28].

Cellular uptake study by confocal microscopy

Cellular internalization of HNCs in A549 cells was assessed by confocal microscopy. Cells were seeded onto 24-well plate at a density of 10^4 cells/well. After 24 h, cells were transfected with ncrCCL-p-HNCs (wherein ncr = FITC-labelled negative control siRNA (FITC-NC-siRNA)), ncrL2K (ncr complexed with lipofectamine 2000) and ncr (FITC-NC-siRNA) at concentration of 100 nM. After incubation period of 6 h, cells were washed with cold PBS and fixed using ice cooled 3.7% paraformaldehyde solution for 5 min. DAPI (1 µg/mL) was used to stain cell nucleus for 10 min. After washing with PBS three times, cover slips were mounted on slides, sealed with glycerine and visualized for cellular uptake using confocal laser scanning microscope (LSM 710, Carl-Zeiss, USA) [29].

Cellular uptake study by flow cytometry

A549 lung carcinoma cells were seeded at a density of 5×10^5 cells per well in 6-well plate. After 24 h proliferation, cells were given treatment with ncrCCL-p-HNCs and ncrL2K, containing FITC-NC-siRNA at 100 nM concentration and incubated for 6 h at 37 °C in 5% CO_2 incubator with humidified air. Then cells were harvested and collected in FACS buffer (0.5% bovine serum albumin and 0.5 mL FBS) and analysed for fluorescence intensity using fluorescence activated cell sorter (FACS-BDAria-III, BD, USA). Naked FITC-NC-siRNA was also evaluated for uptake. FlowJo (BD bioscience, USA) software was utilized to process and analyse the raw data [30]. Quantitative levels of cellular uptake of the formulations were represented relative to unstained cells.

Cell cycle analysis

A549 cells were transfected using rCCL-p-HNCs as described in the cellular uptake method "Cellular uptake study by flow cytometry." The cells were collected, processed and were subjected to FACS analysis to determine progression in cell cycle. CCL-p-HNCs were also studied, and untreated cells were used as control (medium only). Active Ingredient concentration in HNCs was 10 µM equivalent to 3 µg/ml. Cells were trypsinized after 24 h and collected in complete media. Cells were then centrifuged at 2000 rpm at room temperature for 5 min and again resuspended in PBS. About 70% ethanol was used to make cells permeable for PI and cell suspension was left at 4 °C overnight. Cells were subsequently washed with PBS, centrifuged again and resuspended in incomplete media along with 10 µl of RNase. About 5 µl of PI (1 mg/mL stock solution) was also added to this cell suspension and incubated at 37 °C for 1 h prior to analysis through BD FACS Aria III, BD Biosciences, USA [17].

Gene knock-down by RT-PCR

Real-time polymerase chain reaction (RT-PCR) technique was used to quantify mRNA knock-down due to siRNA-mediated transfection and determine the percentage expres-sion levels compared with untreated cells (control). A549 cells were seeded onto 24-well plates at a density of 5×10^4 cells/well for 24 h. Three different concentrations of ABCC3 siRNA were used, i.e. 50 nM, 100 nM and 200 nM to deter-mine the effect of concentration on expression levels. Cells were transfected with rCCL-p-HNCs, Naked siRNA and Lipofectamine 2000 (L2K), and scrambled sequence of siRNA complexed with formulation was used as negative control (ssrCCL-p-HNCs). The untreated control was used to assess the basal gene expression, L2K was used as positive control, whereas NC-siRNA was used to confirm the specificity. After 48 h, total RNA was isolated using the TRIzol reagent (Invitrogen, USA) and reverse transcribed into cDNA using RNA to cDNA conversion kit (Invitrogen, USA). The mRNA level was quantified using Step One real time PCR (Applied Biosciences, USA). Each reaction was performed using SYBR Green Master mix (Applied Bio-sciences, USA), forward and reverse primer, and 2 ng of cDNA in a total volume of 20 µL. The housekeeping gene glyceraldehyde-3-phosphate dehydrogenase (GAPDH) was utilized to normalize mRNA expression level for ABCC3 [31].

In vivo studies

All institutional and national guidelines for the care and use of laboratory animals were followed. The *in vivo* studies were conducted in the laboratory of Department of Pharmacology, Maliba Pharmacy College, Uka Tarsadia University, Bardoli. All animal experiments and protocol described in the present study were approved by the Institutional Animal Ethical Committee (IAEC) of Maliba Pharmacy College, Uka Tarsadia University, Bardoli wide protocol MPC/IAEC/02/2019 and with permission from committee for the purpose of control and supervision of experiments on Animals (CPCSEA), Ministry of Social Justice and Empowerment, Government of India.

Tumour regression study

Tumour regression potential of the formulations (CSol, CCL-p-HNCs and rCCL-p-HNCs) were evaluated in A549 xenograft model in 8-week-old BALB/c nude mice. The tumour that was induced using subcutaneous injection of A549 human lung adenocarcinoma cells ($4 * 10^6$ cells) was given into right flank of mice (6 mice/group). Tumour volume was allowed to reach around 200 mm^3, and the animals were divided randomly in four groups. The above-mentioned formulations were injected through tail vein (IV route) which contained Active Ingredient and ABCC3 siRNA at the dose of 6 mg/kg and 133 µg/kg respectively. The dose was selected based on maximum tolerated dose (data not shown)on the first day of each week for 3 weeks (i.e. at 1st, 8th, 15th and 22nd days). Saline was used as control group. Tumour size and tumour volume were estimated using its dimensional values. Tumour bearing mice were euthanized at the end of 5th week, and tumour were excised and weighed. Graphs of tumour volume and tumour mass were plotted and compared [32–34].

Pharmacokinetic study

Pharmacokinetic profile was estimated in 6–8-week-old female Sprague–Dawley rats according to previously determined methods earlier [35]. Animals were divided into two groups ($n = 6$), and they were injected CSol and rCCL-p-HNC formulations at Active Ingredient dose equivalent to 6 mg/kg through tail vein. Retro-orbital puncture method was used to collect blood samples at predetermined time (0, 0.5, 1, 2, 4, 6, 12 and 24 h) into a heparinized Eppendorf tube. Plasma was separated from blood after centrifugation at 5000 rpm at 4 °C for 10 min. Samples were kept at − 20° °C until further analysis. Estimation of Active Ingredient was performed by validated normal-phase HPLC method (NP-HPLC) (Agilent Tech-nologies 1260 infinity II, USA) using L8 column (Thermo scientific, USA) at ambient temperature. IV Pharmacoki-netic parameters were analysed using Kinetica software 5.1 assuming non-compartmental modelling.

Statistics analysis

Experiments were performed in triplicate. The data are expressed as the mean ± standard deviation (SD) unless stated in the experiments. The statistical significance of the results was determined using a Student's *t* test and one-way analysis of variance (ANOVA) at statistical significance $p < 0.05$.

Results and discussion

Formulation and characterization of CCL-HNCs

Preparation of Active Ingredient caprylate complex

The hydrophilic drug, Active Ingredient, has aqueous solubility of around 2.5 mg/ml. Thus, its entrapment in either the aqueous or the bilayer of lipid vesicles has been limited. One of the strategies to improve the lipid solubility includes complexa-tion with ligand molecules. This would also lead to improve-ment in the partitioning of the drug towards the amphiphilic core of the copolymer. The reaction of Active Ingredient with sodium caprylate is of coordination complexation type, wherein the positive charge attained by the drug in aqueous solution interacts with the negatively charged ligands to form com-plexes. The coordination complex formation was aided by high temperature of the solution and the improvement in complex formation may be attributed to increased kinetic energy of the molecules, leading to enhanced solubilization of drug. The pH of the reaction medium was kept near pKa of the drug which ensured ionization of Active Ingredient. The syn-thesized Active Ingredient-caprylate complex was obtained as a fine white dispersion. The lipophilic nature of formulated drug complex may help in improved drug loading of Active Ingredient in the lipid bilayer and polymeric core as reported earlier. Formation would lead to increase in the lipophilicity of Active Ingredient, which could help in partitioning of the drug more towards the lipophilic bilayer as well as in the polymeric core, thereby increasing entrapment of Active Ingredient in HNCs which consist of lipidic as well as amphiphilic components.

Formulation of CCL-HNCs

The formulated HNCs were prepared by thin film hydra-tion method followed by extrusion. Hydration of the films consisting of lipid mixture and diblock copolymer and self-assembly of PEG-PLA occurs to form a core where after the lipophilic head of lipids orient themselves towards the core and align according to hydrophobic interaction on the surface to decrease free energy of the system and give rise to a stable hybrid system. The components of the system were selected for development of HNCs exhibiting cationic surface charge for siRNA complexation and possessing endosomal escape property. DPPC (glass transition Tg: 41 °C) was selected as the primary film forming lipid around the polymeric core in HNC. Inclusion of cholesterol in HNC was done to impart film elasticity and fluidity. DOPE as a neutral lipid may aid the endosomal escaper of the HNC. Fatty acid carboxyl ions of DOPE make nanocarrier stable at lamellar phase in neutral pH due to electrostatic repul-sion, but at acidic pH inside the endosome, these groups get protonated, converting them into the unstable hexagonal phase which in turn fuse, aggregate and release the cargo into the cytosol easily. Furthermore, DOTAP was added to provide cationic charge to HNCs for effective complexation of negatively charged siRNA. The schematics of the forma-tion of HNCs have been presented in Fig. 1, and it may be assumed that physicochemical or interfacial properties of the formulated polymeric core-lipidic shell type of HNC may be similar to those reported earlier [18, 19]. Importantly, hydration of the lipo-polymeric film above glass transition temperature of lipid mixtures would assist in self-assembling of the lipids around the polymeric core in HNC formation similar to that of the conventional lipid-based systems [36]. The surface coating using DSPE-PEG molecules provided stealth outer layer to HNCs leading to improved circulation time and stability upon intravenous administration [37].

Size, zeta potential, entrapment efficiency and drug loading

The results of size distribution, zeta potential, entrapment efficiency and drug loading of drug loaded liposomes as well as various batches of drug-loaded non-PEGylated and PEGylated HNCs are presented in Table 1. Batches V1 to V3 (non-PEGylated) were screened to evaluate effect of addition of copolymer and cationic lipid to the lipid composition on the tested parameters. These batches exhibited size in the range of 120–140 nm. The entrapment efficiency of Active Ingredient caprylate in liposomes of batch V1 was found to be 35.3 ± 3.5% which may be attributed to drug loading in lipidic layer compart-ment of liposomes. High-speed centrifugation was used to separate the free Active Ingredient caprylate from the HNCs. This method was evaluated by achieving mass balance through measurement of unentrapped drug in sediment and entrapped drug in supernatant containing HNCs. Batch V2 and V3 were prepared with block co-polymeric component along with the lipid components and exhib-ited improved entrapment efficiency of 65.6% and 68.5% respectively. The increment in drug loading from 0.07 to 0.21 mg was also observed due to incorporation of copolymer in the composition whose amphiphilic prop-erty would lead to partitioning of the drug in the core over and above that in lipid bilayer. One thing to note is

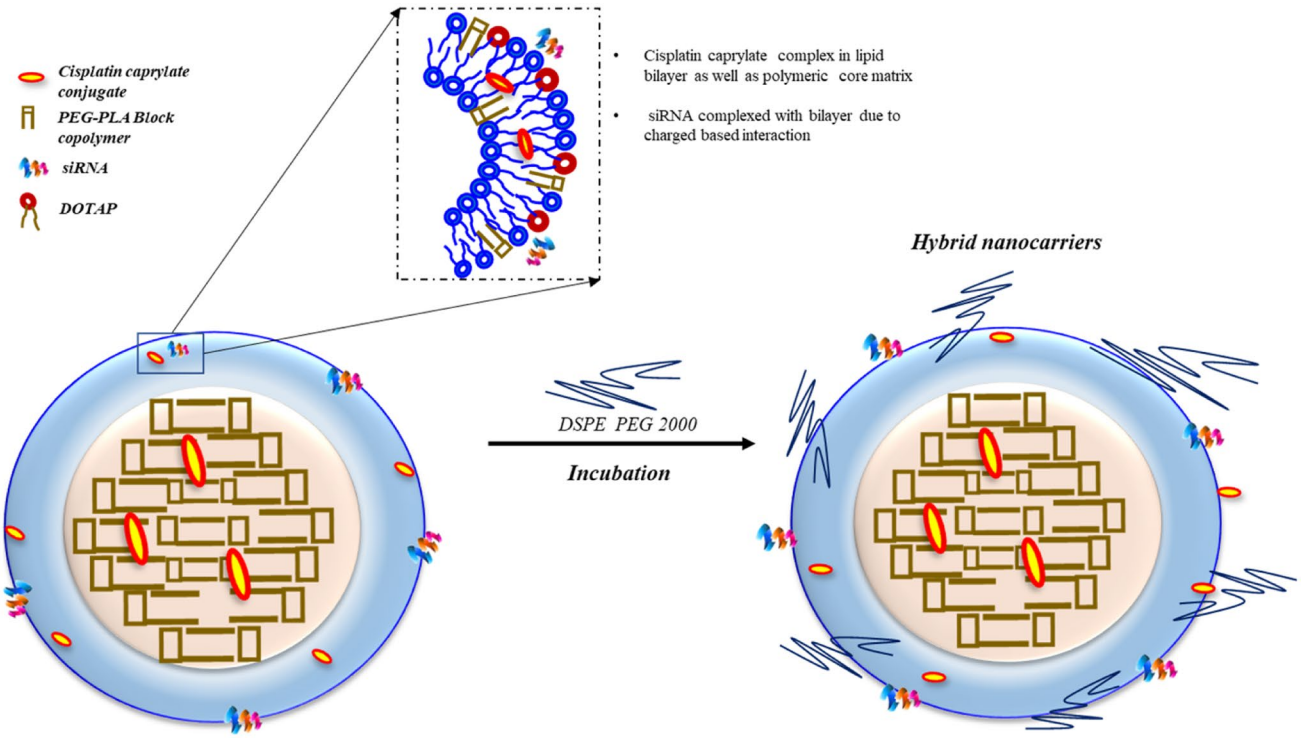

Fig. 1 Schematic of hybrid nanocarriers (HNCs)

that these batches were prepared without addition of cholesterol; hence, the overall fluidity of membrane would be less to tolerate the shear during processing leading to lesser drug entrapment as opposed to our previous findings as well as were prepared using film hydration technique instead of emulsion solvent evaporation method leading to comparatively lower entrapment values [16]. Evaluation of the sedimented pellet after centrifugation confirmed these speculations (data not shown). Effect of variation in lipid to polymer (L/P) weight ratio was evaluated by changes in size and entrapment of the formed HNCs in batches V4 to V7. Batch V4 showed a particle

Table 1 Effect of lipid-polymer content on HNCs

Batch	Composition of formulation	Size(nm)	PDI	Zeta potential (mV)	Drug entrapment(%)	Drug loading*(mg)
V1	DPPC:DOPE:DOTAP—6:2:2 (5 mM)	121.6 ± 1.5	0.18 ± 0.03	42.81 ± 1.59	35.3 ± 3.5	0.07
V2	DPPC:DOPE—3:1 (5 mM),PEG-PLA (5 mg/mL) and L:P—3:1 w/w	134.3 ± 1.9	0.15 ± 0.03	22.47 ± 0.89	65.5 ± 4.9	0.20
V3	DPPC:DOPE:DOTAP- 6:2:2 (5 mM), PEG-PLA and L:P—3:1 w/w	128.9 ± 1.4	0.14 ± 0.02	42.91 ± 1.67	68.2 ± 3.8	0.21
V4	DPPC:Cholesterol:DOPE:DOTAP-6:2:1:1 (5 mM), PEG-PLA (5 mg/ml) and L:P—3:1 w/w	153.8 ± 1.6	0.15 ± 0.03	38.16 ± 0.79	84.9 ± 2.2	0.29
V5	DPPC:Cholesterol:DOPE:DOTAP-4:4:1:1 (5 mM), PEG-PLA (5 mg/ml) and L:P—1:1 w/w	141.4 ± 2.8	0.47 ± 0.06	18.52 ± 1.75	55.7 ± 3.8	0.18
V6	DPPC:Cholesterol:DOPE:DOTAP-6:2:1:1 (10 mM), PEG-PLA (5 mg/ml) and L:P—4:1 w/w	200.1 ± 5.5	0.48 ± 0.08	35.63 ± 0.59	40.9 ± 2.6	0.26
V7	DPPC:Cholesterol:DOPE:DOTAP-4:1:1:1 (5 mM), PEG-PLA (5 mg/ml) and L:P—1:3 w/w	148.7 ± 3.2	0.53 ± 0.05	12.58 ± 0.78	42.5 ± 2.9	0.20

PEG−PLA at 5 mg/mL; L:P—lipid to polymer ratio (w/w). *Per milligram of solid (lipid + polymer), average values are reported. #Post-insertion technique was used to incorporate DSPE−PEG 2000 (3 mol % of total lipid contents) in V4 to V7. Values reported are mean ± SD unless specified

size of 153.8 nm with marginal increment which may be attributed to post-insertion of the PEGylation layer. However, the formulation presented similar entrapment effi-ciency of Active Ingredient caprylate as that of batch V3. These changes in entrapment may be attributed to addition of cholesterol in the lipid composition. Conversely, reduc-ing the L/P ratio along with increasing the cholesterol content (Batch V5) resulted in the quality of HNCs. This observation substantiates the importance of lipid compo-sition during PEGylation impacting packing character-istics and thus PDI [38]. It was observed that the size of HNCs was significantly increased above 200 nm along with high polydispersity index when L/P weight ratio was kept higher (4:1, BatchV6) with increase in lipid con-centration to 10 mM. Furthermore, if L/P ratio was low (1:3% w/w, Batch V7), higher PDI value was obtained indicating unfavourable balance of hydrophilic and hydro-phobic groups between lipids and polymers which may lead to aggregation due to insufficient lipid coating. Zeta potential value was found to be decreased (~ 12 mV) in such cases with lower L/P ratio. There was decrease in entrapment of Active Ingredient caprylate in batches V5 and V7 which indicated effect of L/P ratio on drug entrapment efficiency and drug loading. As polymer weight ratio increased, drug entrapment was found to decrease which may be due to insufficient lipid coating which also presents space for drug in the bilayer compartment [39]. The finalized composition for further evaluation was batch V4.

In vitro drug release study and release kinetics

The release profile of optimized formulation CCL-p-HNCs (batch V4) tested in various media are presented in Fig. 3. The drug release at pH 7.4 was found to be low (20%) after 12 h with only 33% being released after 96 h (Fig. 2a). Drug release at pH 6.6 was found to be similar to that of pH 7.4 with 25% and 48% drug release after 12 h and 96 h respectively. However, significant increase in drug release profile was observed at pH 5.5 with an initial burst release of 41% after 12 h and 73% after 96 h. The results of drug release indicated low drug Active Ingredient release in blood and normal tissues with reduced toxicity during transit to tumour cells post-intravenous administration of the CCL-p-HNCs. Further, release profile at pH 5.5 indicated the site-specific drug release in the endosomes and lysosomes of cancer cells after the uptake of the HNCs by EPR effect leading to chances of improved efficacy in reduction of tumour load. Importantly, the drug release would invari-ably be affected by the rates of the drug release from both the polymeric core and the lipid bilayer. Consequently, we studied the drug release kinetics using various models

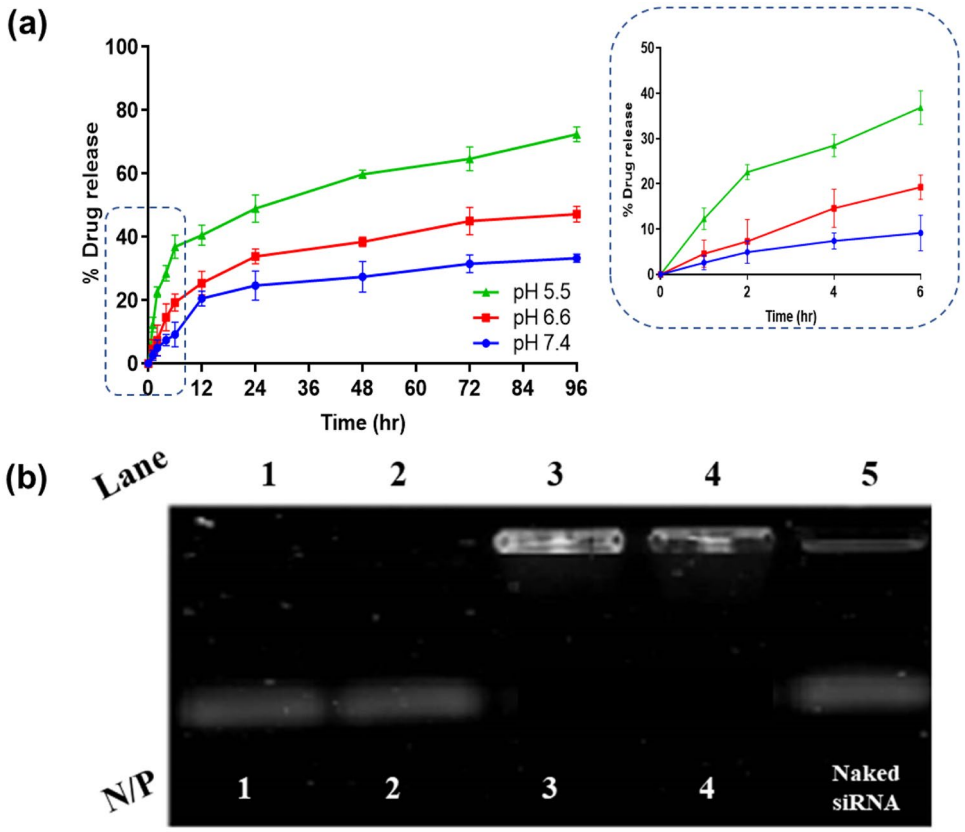

Fig. 2 **a** Active Ingredient caprylate release from drug loaded HNCs at different pH. **b** Gel retarda-tion assay coloaded HNCs at different N/P ratio

(data not shown). The results suggest diffusion controlled drug release from CCL-p-HNCs (Higuchi model, highest $R^2 = 0.9844$). However, studies are further required to confirm exact mechanism due to complex nature of formu-lation. We anticipate the hydrolytic stability of Active Ingredient caprylate complex could be similar to that reported earlier using ^{195}Pt NMR spectroscopy [40] for ligands complexed to drug.

Formulation and characterization of rCCL-p-HNCs

Formulation of rCCL-p-HNCs and complexation efficiency of siRNA

The complexation of siRNA with CCL-HNCs was achieved using charge-based interaction between cationic lipid DOTAP and anionic siRNA with incubation time being optimized. Incubation time for the maximum complexation efficiency between siRNA and pre-formed HNCs was optimized. The mixture was gently vortexed for 2 min and incubated for different time points (10, 20, 30, 60 and 120 min) at different temperature conditions (5° to 35 °C, with increment of 10 °C). Maximum siRNA-HNC complexation was obtained with incubation time of 30 min and temperature of 25 °C (data not shown). These optimum parameters were selected for further formulation of batches of rCCL-p-HNCs. Further, it was observed that N/P ratio < 3 was associated with high content of free siRNA which migrated towards positive end of electrode on agarose gels. Lack of complete complexation may result in the loss of siRNA before entering the cell and/or may result into its inactivation during circulation. However, complete complexation was found to have occurred at N/P ratios of 3 and 4, which were indicated by visible band, confirming absence of migration of siRNA on agarose gel (Fig. 2b). Thus, the absence of free siRNA N/P of 3 and 4 indicated complete complexation of siRNA at these N/P ratios (Table 2) [41]. The results indicated that at lower N/P ratio (Batch B2 and B3), the complexation efficiency of siRNA was less (35%), whereas for N/P ratio of 3 and 4 (Batch B4 & B5), it was higher (> 90%). The N/P ratio of 3 was selected for further evaluation.

Size and zeta potential measurement

The changes in the size due to PEGylation along with change in zeta potential due to complexation with siRNA have been presented in Table 2. Post-insertion technique of PEGylation slightly increased the particle size for all the batches B1 to B5, which may be attributed to increase in the hydration volume on the surface. Additionally, the particle, size would have been dependent on the chain length of PEG-lipid [42]. Zeta potential was found to be significantly decreased after siRNA complexation and suggested the surface interaction between positively charged HNCs and negatively charged siRNA [12, 43]. The results of zeta potential of non-PEGylated HNC formulation complexed with siRNA (batch B6) (non-PEGylated batch, complexed with siRNA), the complexation resulted in decreased values from 50 to 36 mV. Similar decreased values were observed in the PEGylated formulation (B1 to B5). These results indicated that PEGylation of the HNCs not only increased the hydrodynamic diameter of the carrier of the carrier but also changed the surface potential with chances of charge based shielding of HNC core similar to that previously reported [44, 45]. Further, zeta potential values of formulated HNCs that were on positive side would result in charge-based interactions with the negatively charged cell membrane.

Cryo-TEM and freeze fracture TEM studies

Morphological evaluation of rCCL-p-HNCs done by cryo-TEM revealed the uni-lamellar structure with particle size of less than 200 nm (around 160 nm) consistent with that obtained using DLS. This size range is expected to assist

Table 2 Characterization of coloaded HNCs

Batch	N/P ratio	siRNA % complexation efficiency	Effect of PEGylation on particle size (nm)		Effect on siRNA complexation on zeta potential (mV) of CCL-p-HNCs	
			Before PEGylation	After PEGylation*	Before complexation	After complexation
B1	NA	NA	132.2 ± 0.11	147.4 ± 1.79	38.16 ± 1.49	21.79 ± 0.79
B2	1	34.78 ± 3.46	145.6 ± 0.86	160.5 ± 0.89	41.79 ± 0.67	25.93 ± 0.49
B3	2	43.95 ± 4.18	128.2 ± 1.59	147.9 ± 0.16	48.37 ± 1.69	27.29 ± 1.73
B4	3	95.83 ± 2.39	139.9 ± 0.45	153.2 ± 1.76	47.97 ± 0.49	25.39 ± 0.49
B5	4	92.69 ± 2.76	132.2 ± 0.78	148.8 ± 0.79	53.61 ± 0.73	22.61 ± 1.79
B6[#]	3	90.36 ± 3.83	133.4 ± 1.59	NA	49.95 ± 1.49	36.56 ± 2.10

All batches B1 to B6 have similar formulation composition as Batch V4 mentioned in Table 1

#B6 was formulated without addition of DSPE PEG 2000; *along with siRNA

in EPR effect for tumour internalization of nano-carriers. Formation of distinct PEG-PLA matrix core in HNCs was confirmed through the TEM image wherein a dense region inside the lipid outer membrane. To further confirm the morphology of the formulation and assess the presence of coating around the core, freeze fracture TEM was carried out [46]. As evident, the morphology observed complemented the results observed in cryo-TEM, wherein the solid polymeric core was clearly visible upon fracture of the plane which is surrounded by a lipid bilayer and had spherical structure (Fig. 3 a and b).

Atomic Force Microscope (AFM) Analysis

The atomic force microscope (AFM) system has evolved into a useful tool for direct measurements of micro-structural parameters and unravelling the intermolecular forces at nanoscale level with atomic-resolution characterization. AFM measures surface morphology and properties. The main advantage of the technique is the possibility to operate in real-time and at the nano-meteric scale. The morphological studies of rCCL-p-HNCs performed by AFM showed uniform and spherical shaped discrete particles (Fig. 4a) without aggregation with approx. size of 150 nm. The height histogram (Fig. 4b) shows fairly narrow distribution of peak heights from 5 to 20 nm indicating presence of PEGylation layer [47].

Small angle X-Ray scattering (SAXS) study

HNC shape and architecture rCCL-p-HNCs (Batch B4) in three dimensions were analysed through SAXS. Results of experimental data are given in Fig. 4c. The data were transformed into an inter-atomic vector distribution profile (Fig. 4d) which revealed 142 nm of maximum dimension and 71 nm of radius of gyration thereby confirming spherical shape of HNCs [48]. Variation of scattering curve intensity indicated the complexity of internal structure of nanocarrier system. Intersection of all scattering curves at one point was defined as the iso-scattering point related to the external radius of the particle which was inaccessible to solvent. Further iso-scattering point was located at $q = 0.213\ \text{nm}^{-1}$ which corresponded to radius of 71 nm and diameter of 142 nm. These results of particle size of HNCs were not significantly different from that obtained by DLS. Moreover, shape of the nanocarrier system was also revealed by shape factor model fitting [23].

Integrity of siRNA by serum stability study

In post-systemic administration, the formulation would have come in direct contact with blood consisting of serum with nuclease enzyme that might deactivate the siRNA. Such inactivation of siRNA would not lead to loss of activity in the cells after reaching the site leading to therapeutic failure. Thus, it was important to verify the intactness of the siRNA in the formulation. Figure 5 a presents the gel electrophoresis image of naked siRNA at various time points. As evidenced from the band densitometric analysis, the naked siRNA showed rapid degradation in the presence of serum within 30 min and only 20% of siRNA remained intact at the end of 8 h as compared with initial loading. Such results were not observed with the formulations. From the results of band density analysis by gel electrophoresis and nanodrop (Fig. 5 b and c), it may be concluded that HNCs with PEGylation retained integrity of siRNA in the serum higher than that to non-PEGylated HNCs. This may be attributed to the presence of PEGylation layer on the HNCs that provided steric hindrance while protecting the siRNA from contact with serum components. These results were consistent with the reported effects of post-insertion technique of PEGylation which provided the advantages of coating with good encapsulation and protection of nucleic acid in blood [43]. It further fulfilled the requirements of being able to retain an efficient delivery of siRNA/drugs to cancer cells and led to reduced premature siRNA release [25]. HNC encapsulated siRNA were found to be stable after 24 h with more than 70% of siRNA being detected on agarose gel. These results confirmed that prepared HNCs would efficiently protect the encapsulated siRNA in the serum for period of 24 h post-systemic administration.

In vitro cell line study

Cytotoxicity studies by MTT assay

The results of MTT studies are depicted in Fig. 6a to c along with IC_{50} values in Table 3. The MTT assay for blank formulation displayed less than 10% cell death at highest concentration tested, indicating the non-cytotoxic nature of the carrier (data not shown). The cytotoxicity displayed by CSol and CCL-p-HNCs at various concentration and time were quite similar and changes in IC_{50} of later with respect to former were only 1.04, 1.18 and 1.03 at 24 h, 48 h and 72 h respectively. This indicated that CSol and CCL-p-HNCs were presented equivalent amount of drug to the cells. Further, a probable reason for non-improvement in the cytotoxicity would be due to the slow release of drug from the formulation due to sustained release characteristics and is consistent with the results reported in studies earlier [49, 50]. The most significant effect on cell viability profile was observed with rCCL-p-HNC formulation, wherein a 3.35-fold improvement in IC_{50} value was observed at 72 h. This reduction in value may be attributed to the impact of siRNA on the drug efflux inhibition. The IC50 values

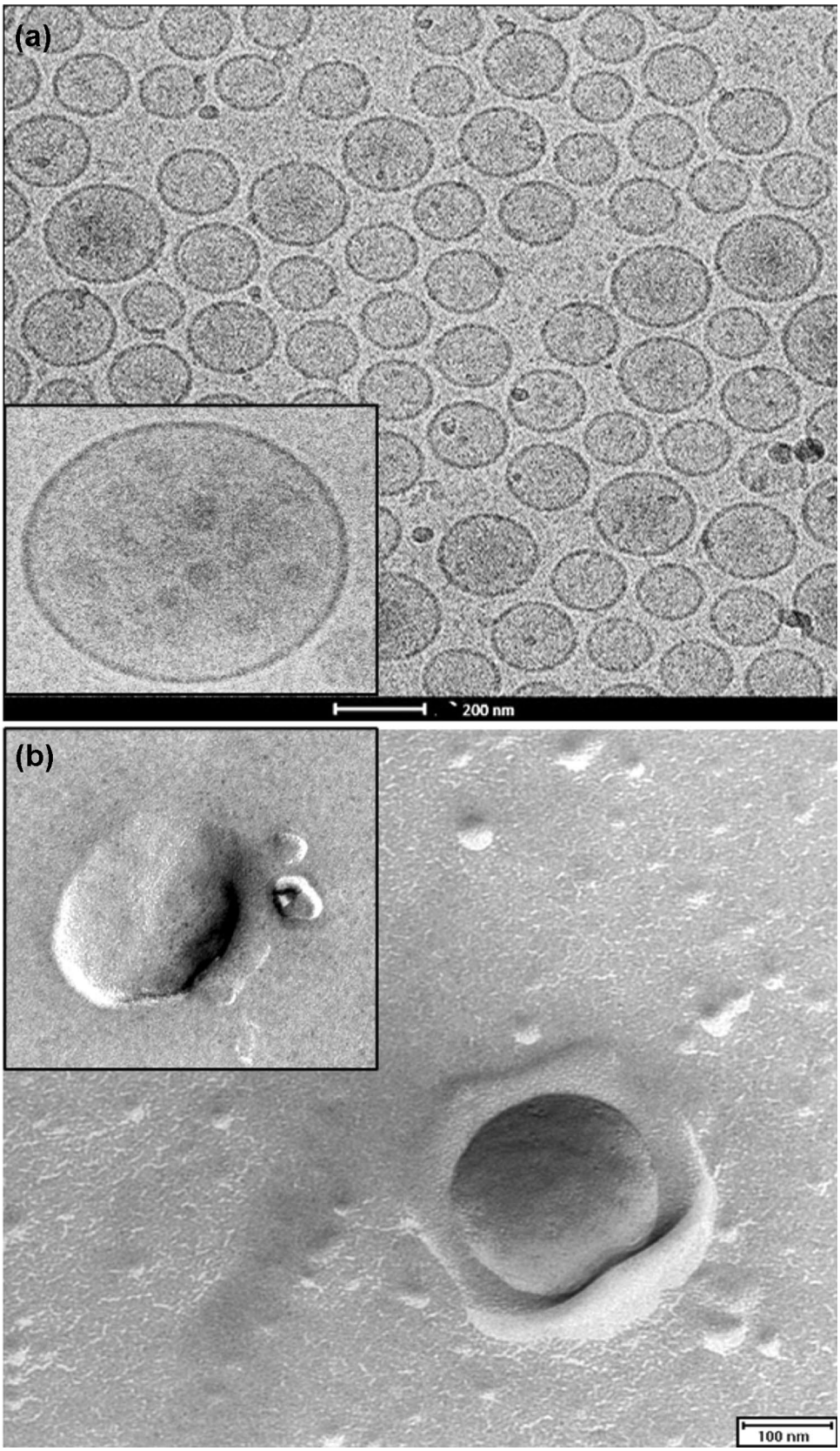

Fig. 3 **a** Cryo-TEM of coloaded HNCs. **b** Freeze fracture TEM for coloaded HNCs

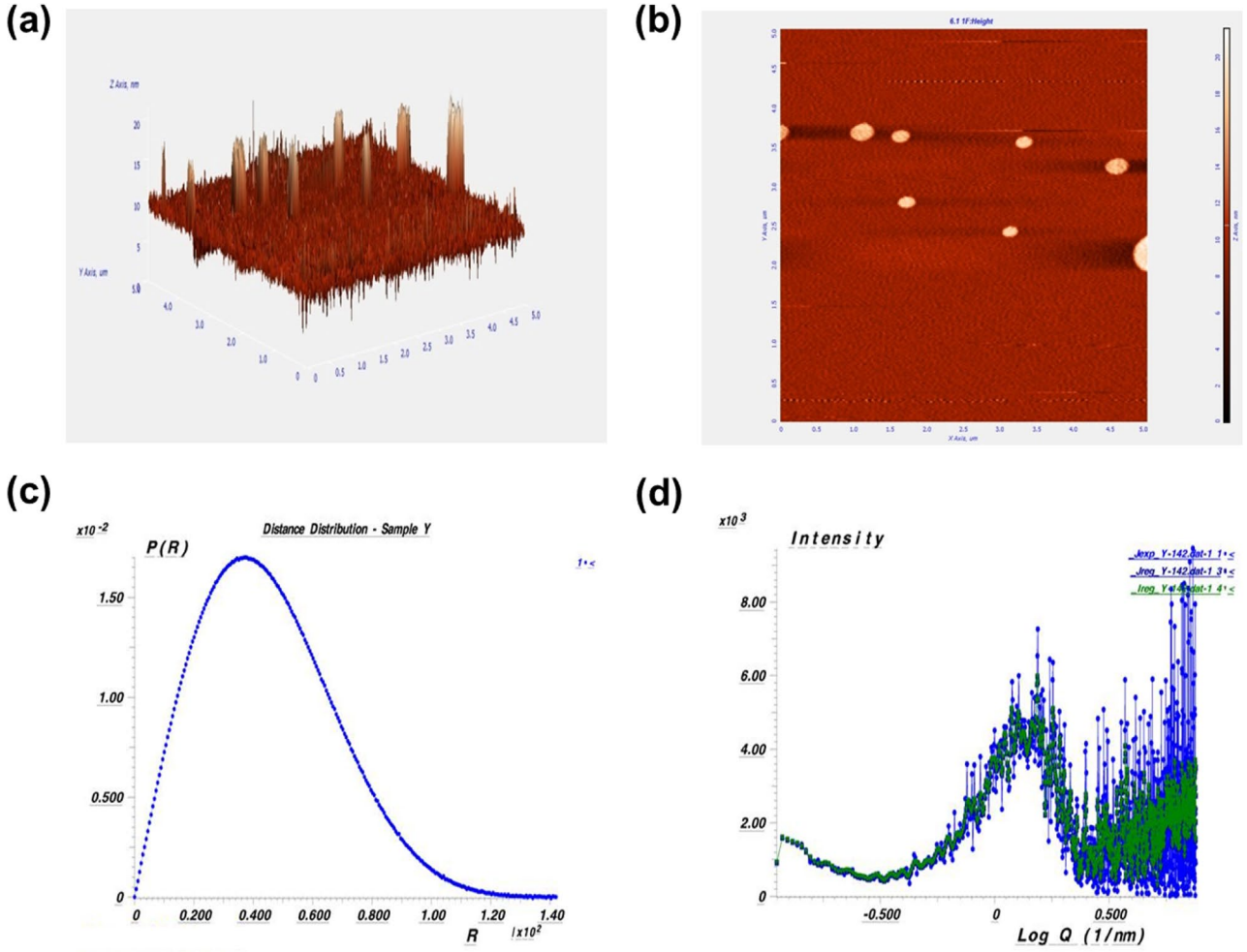

Fig. 4 **a** Atomic force microscopy (AFM) of drug loaded HNCs, **b** AFM histogram of drug loaded HNCs, **c** SAXS 3D modelling and **d** SAXS inter atomic vector distribution profile for drug loaded HNCs

after rCCL-p-HNC treatment at 24 h and 48 h, resulted in 1.57- and 2.27-fold reduction respectively. A549 cell lines have been reported to have expressed ABC efflux pumps that readily efflux the various chemotherapeutics including Active Ingredient from the cells [51]. Thus, co-deliver-ing siRNA would have led to higher cellular level of Active Ingredient for tumoricidal effects due to synergistic effect of co-loading. It may be anticipated that the cytotoxicity to the cells observed herein could favourably be replicated in *in vivo* study in animal tumour xenograft models due to characteristics this formulation possesses for selective extravazation in tumour cells that would occur by enhanced permeability and retention effect (EPR effect) and passive uptake by cancer cells without adversely affecting the normal cells [52].

Qualitative uptake studies using confocal microscopy

Confocal microscopy images of the cell uptake studies were shown in Fig. 7a. It depicted the cellular uptake of ncrCCL-p-HNCs in comparison to ncrL2K and naked FITC-NC-siRNA (ncr). A reduced level of fluorescence was observed in case of cells treated with FITC-labelled naked siRNA indicating inefficient transfection in native state, while for cells treated with HNC formulation, intense fluorescence was observed in the cytosol inside the cells which indicated that the formulation would have been internalized by endocytosis and after counteracting the drug resistance pathway. The release of siRNA in the cytosol would have been triggered after the endosomal escape of HNCs due interaction of cationic outer lipid layer in the HNCs and the negatively charged endosomal membrane by ion pairing

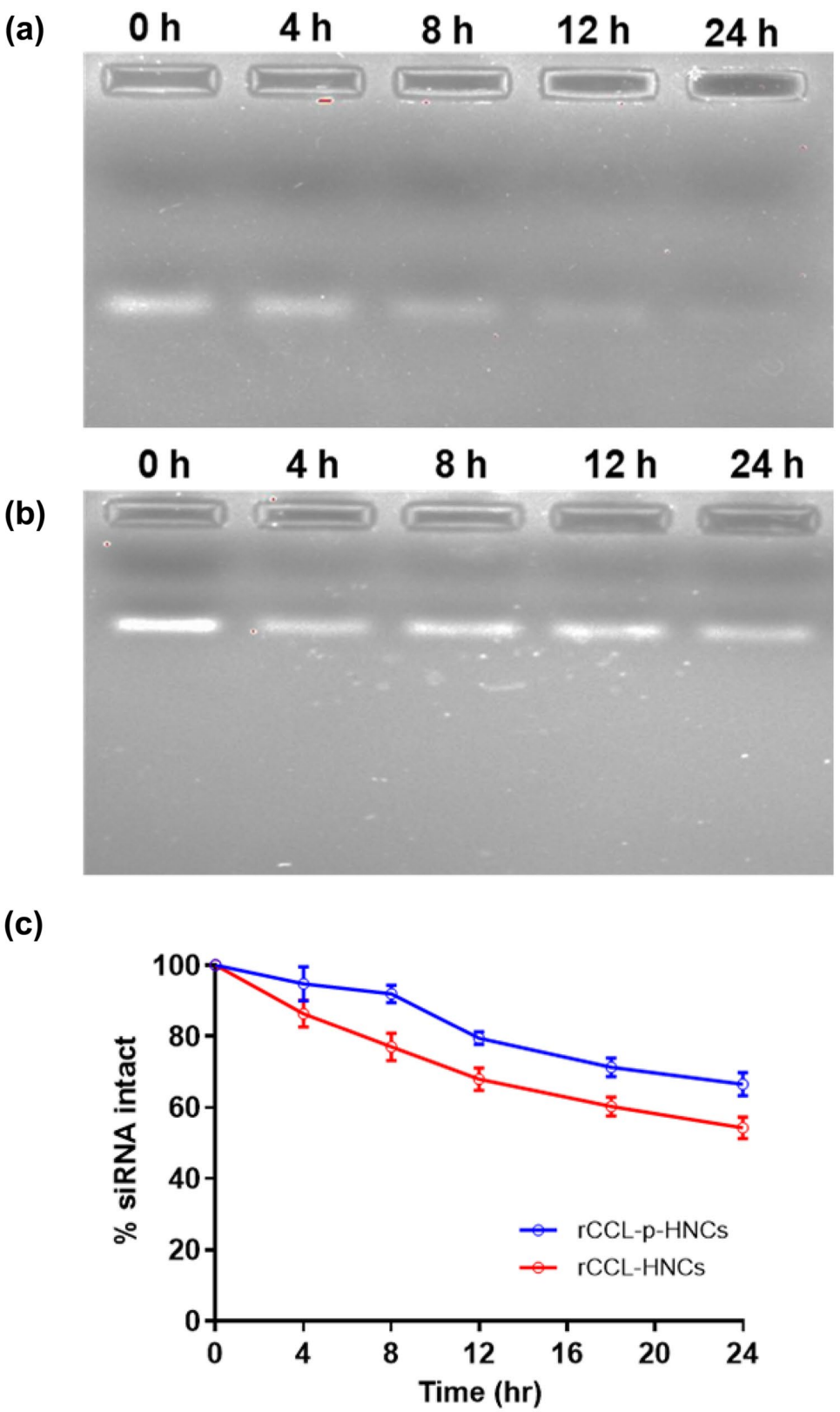

Fig. 5 **a** Serum stability by gel electrophoresis for naked siRNA. **b** Serum stability by gel electrophoresis for PEGylated coloaded HNCs. **c** % siRNA intact vs time for coloaded PEGylated vs non-PEGylated HNCs by nanodrop

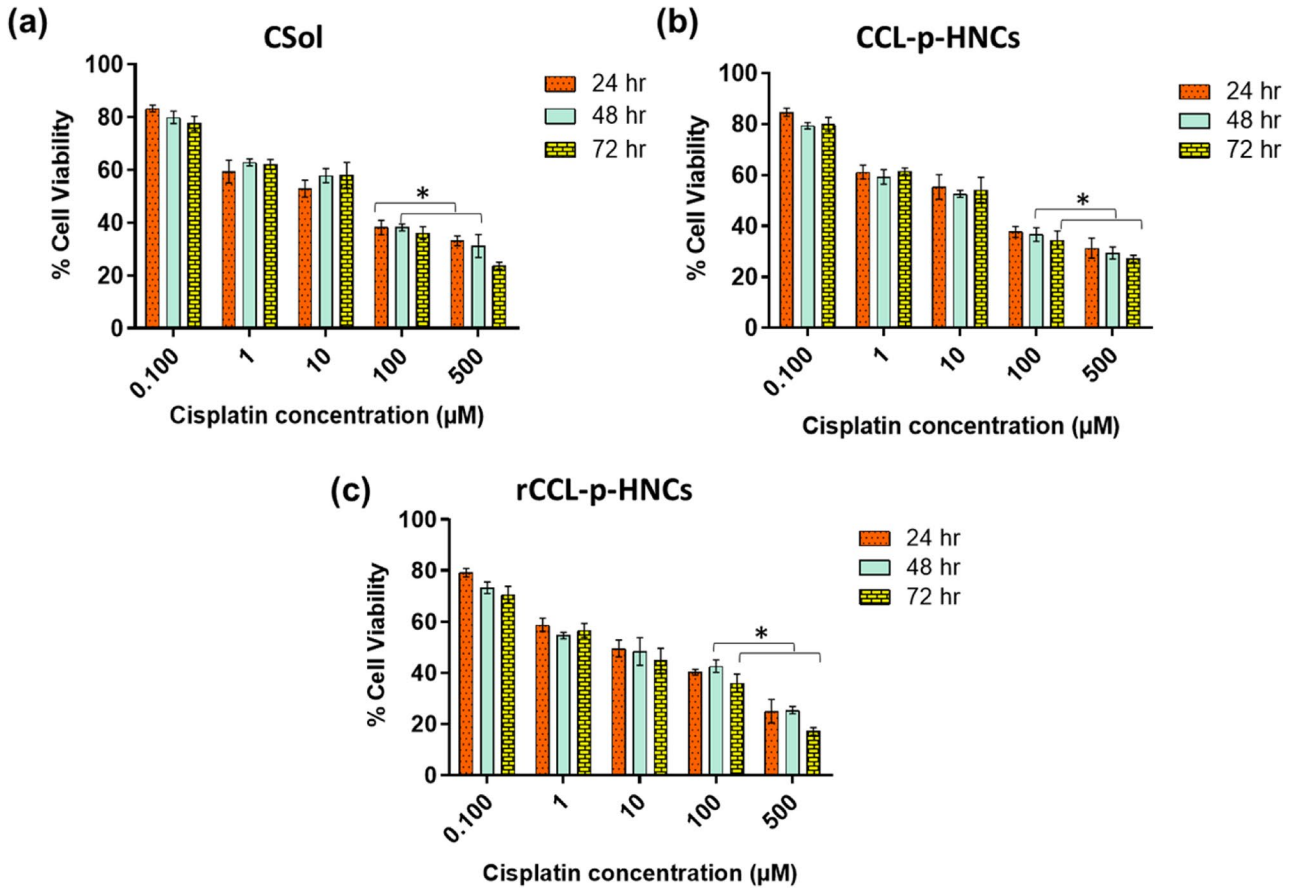

Fig. 6 **a** MTT for Active Ingredient solution, **b** MTT for Active Ingredient loaded HNCs (CCL-p-HNCs) and **c** MTT coloaded HNCs (rCCL-p-HNCs)

leading to endosomal destabilization [53]. Merged confocal image clearly demonstrated that the uptake of formulation into cytosol is comparable to that observed for lipofectamine and it may be concluded that HNCs may deliver the formulation into the cytosol.

Quantitative uptake studies using Flow cytometry

The results of cellular uptake studies by FACS (overlay and relative uptake) of ncr (FITC-labelled naked siRNA), ncrCCL-p-HNCs and ncrL2K were presented in Fig. 7 b and c. It was observed that the ncr showed significantly less geometric mean fluorescence intensity (MFI) (~ 8%) which indicated very marginal transfection efficiency. This result may be attributed to the fact that siRNA would have been degraded by serum nucleases before being uptake and consequently exhibited low fluorescence when observed under confocal microscopy. A significant increase in the MFI was observed with ncrCCL-p-HNCs, which further showed non-significant difference compared with transfection standard lipofactamine-2000 (~81%). Transfection of the cells using HNCs thus depicted that they would be effectively up-taken by the cells and deliver the payload inside the cells to improve the chemotherapeutic efficacy [54].

Table 3 IC_{50} values

Formulation	IC_{50} (μM)		
	24 h	48 h	72 h
CSol	14.92	13.18	11.11
CCL-p-HNCs	14.41	11.20	10.79
rCCL-p-HNCs	9.48	5.81	3.32

Cell cycle analysis

Cell cycle analysis on A549 cells was performed using FACS to determine the impact of rCCL-p-HNCs on cell cycle progression. A comparative evaluation of CCL-p-HNCs was carried out to evaluate the effect of co-loaded formulation on drug efflux pathway. Reports suggest that cell population in a specific cell division stage is proportional to the amount of DNA present in the cell. Cell cycle analysis graph were generated, and the results were represented as cell populations at different stages

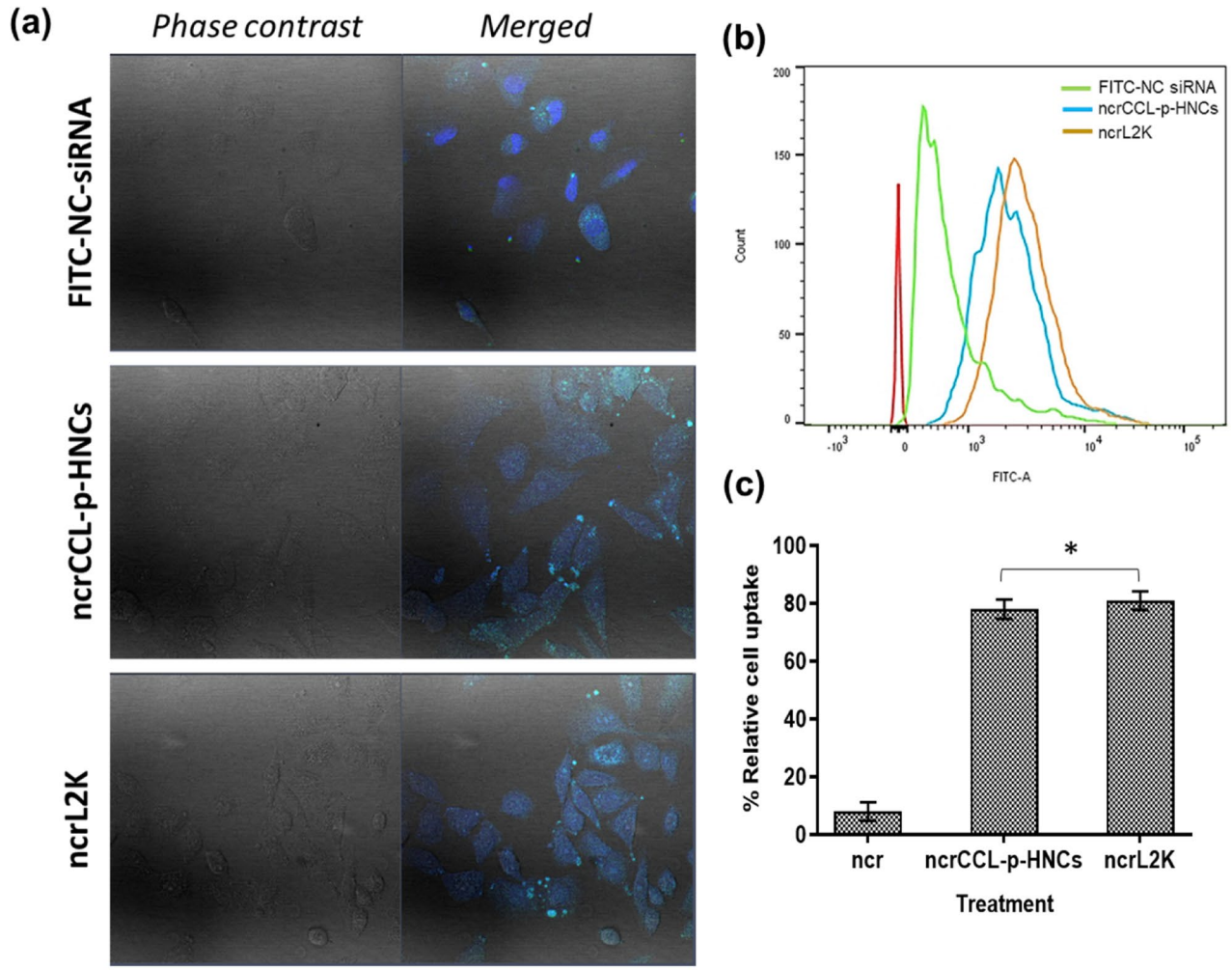

Fig. 7 **a** Uptake study by confocal microscopy. **b** Cellular uptake by flow cytometry. **c** Relative cellular uptake for coloaded HNCs

of cell division. A majority fraction of untreated control cells were observed in G0–G1 stage, whereas for treatment groups, less than 35% were observed in this phase which indicated their progression and cell cycle arrest in G2-M stage. From Fig. 8a it can be seen that there was tremendous increase in the num-ber of cells in G_2-M phase for coloaded HNCs and Active Ingredient loaded HNCs which were 47% and 38% respectively compared with control group which showed around 17% cells. However, the fraction of cells presented in S phase for all three treatment groups showed no significant difference. Our results are partly correlated to the previously published literature wherein Active Ingredient is established to arrest cells in G2-M phase, despite some other suggesting it having non-specific inhibitory actions. The fraction of cells in sub-G1 phase was almost three-fold higher in both treatment groups compared with control group which indi-cated increased apoptotic cell population. These results indicated the significant improvement afforded by co-loading approach on tumour cells which resulted in increased cell cycle arrest as well as improved apoptotic potential.

Gene knock-down by RT PCR

Successful transfection of cell line by formulation would suggest that the payload has been delivered to the cells for exhibiting therapeutic effects. Based on the above *in vitro* studies, the formulations with different concentrations of mRNA were subjected to rt-PCR analysis to estimate its expression level against control cells. The negative control siRNA loaded HNCs did not inhibit the gene expression level, which confirmed the specificity of siRNA sequence selected. For all other treatment groups, a concentration-dependent gene expression inhibition was observed (Fig. 8b). The naked siRNA reduced mRNA expression to a very low extent, while lipofactamine-2000 (L2K) 66% knock-down efficiency was observed at highest concentration tested. Transfection of cell with 100 nM and 200 nM siRNA loaded HNCs strongly downregulated the ABCC3 concentration as evidenced from the percent expression level of gene that was found around 37% and 25% respectively. For 50 nM, the level of downregulation was very low, with 70% activity observed.

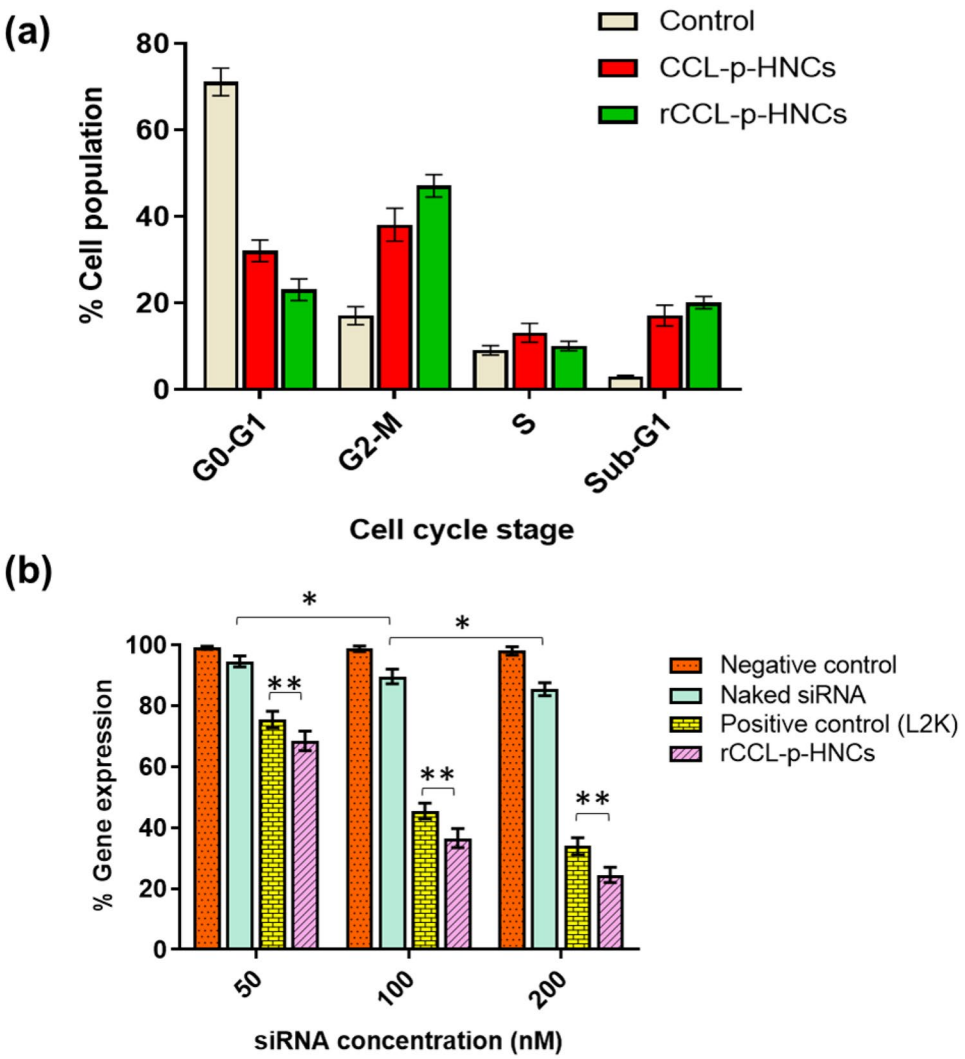

Fig. 8 **a** Cell cycle analysis for coloaded HNCs. **b** Gene expression study by RT-PCR for negative control (scrambled siRNA), naked siRNA, transfection standard (L2K) and coloaded formulation (rCCL-p-HNCs); (**$p < 0.01$)

However, HNCs containing > 100 nM siRNA exhibited a suppression of more than 65% of ABCC3 gene expression. These results may be attributed to the endosomal escape of the formulation after endocytosis and release of siRNA in cytosol.

In vivo studies

Tumor regression study

The therapeutic efficacies of prepared formulations were confirmed by tumour regression study in xenograft tumour model in mice. Treatments were given after achieving predetermined tumour volume approximately 10–15 days after tumour cell inoculation. As depicted in Fig. 9a, delivery of CSol (6 mg/kg) controlled tumour growth up to certain extent. Despite doses injected weekly, there was a gradual continuous increase in the tumour volume. This may be due to the short residence time and rapid elimination from the systemic circulation. Further after the dosing period was completed (i.e. in 4th and 5th weeks), there was rapid increase in the tumour mass. CCL-p-HNCs demonstrated relatively superior tumour growth inhibition and the effect continued even after dosing period was completed. The most significant tumour regression was observed for rCCL-p-HNCs as compared with other treatment groups. The results indicated non-significant change in tumour volume over the entire study period The result of measurement of individual tumour weight (Fig. 9b) substantiated the effectiveness of the coloaded formulation. The significant anti-tumour effect may be attributed to co-loading of ABCC3 siRNA and Active Ingredient. The data had been ana-lyzed by one-way ANOVA. There were significant dif-ferences among formulation treatment groups (CCL-p-HNCs & rCCL-p-HNCs) in comparison to saline and CSol. After cellular uptake and successful endosomal escape, nanocarrier reaches the cytoplasm and release the cargo. RNA interference (RNAi) machinery is present in

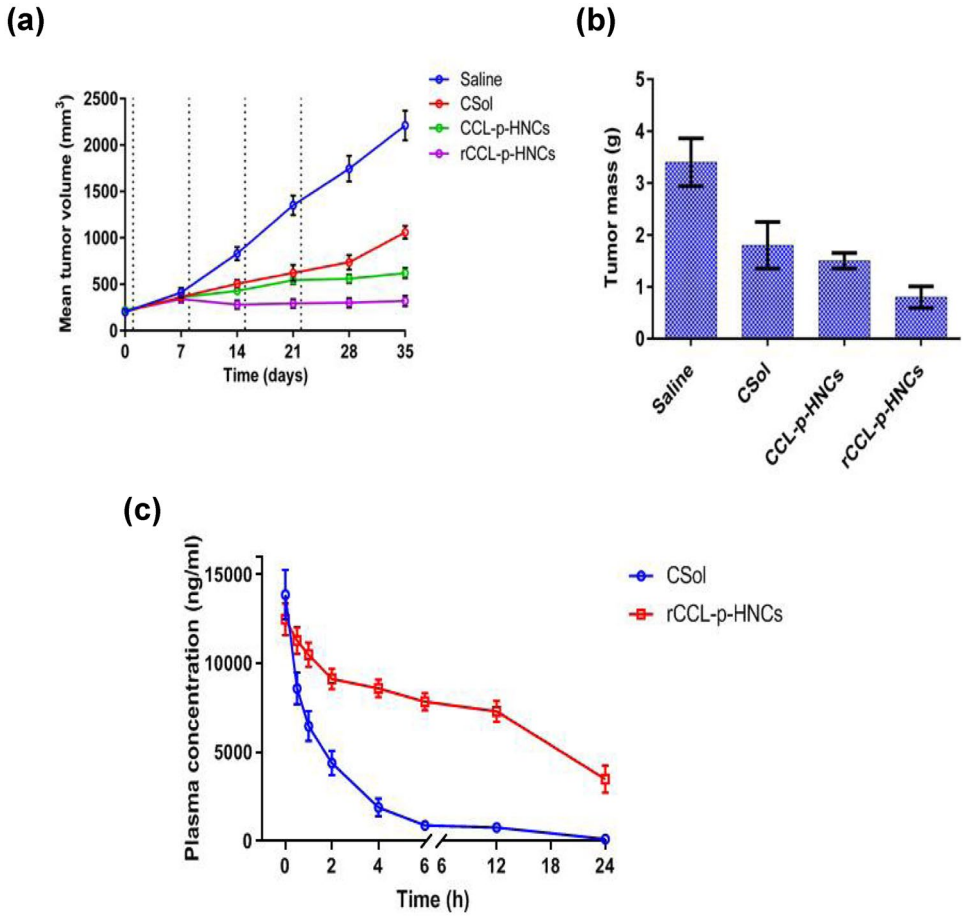

Fig. 9 **a** Tumour regression study in mice usingA549 cell line (dotted vertical line indicates dosing day). **b** Tumour weights. c Pharmacokinetics profile of Active Ingredient in Sprague–Dawley rats from various formulations (CSol and rCCL-p-HNCs)

cytoplasm. Subsequently, siRNA-driven knock-down of efflux protein (ABCC3) prevented Active Ingredient efflux which in turn enhanced chemotherapeutic efficacy of the rCCL-p-HNCs. The enhanced anti-tumour efficacy might be due to long circulation time caused by surface pegyla-tion and ideal nanocarrier size. PEGylation prevents the reticulo-endothelial system recognition and reduced liver and spleen uptake which allows longer blood circulation time. Nanocarrier size less than 200 nm passively tar-gets tumour due to enhanced permeability and retention (EPR) effect [55, 56].

Table 4 Pharmacokinetic parameters of Active Ingredient obtained after single IV dose of rCCL-p-HNCs and Active Ingredient solution (CSol) in Sprague–Dawley rats

Pharmacokinetic parameter	CSol	rCCL-p-HNCs
$t_{1/2}$ (h)	1.46 ± 0.21	35.96 ± 1.93
AUC_{total} (h * µg/ml)	22.78 ± 3.69	297.15 ± 15.22
MRT (h)	2.20 ± 0.26	50.10 ± 0.58
Cl (ml/kg * h)	263.40 ± 48.66	20.19 ± 2.05
V_{ss} (L/kg)	0.58 ± 0.09	1.01 ± 0.11

Values presented as mean ± SD (where $n = 6$)

Pharmacokinetic study

The plasma concentration–time profile of Active Ingredient fol-lowing single IV dose of Active Ingredient solution and rCCL-p-HNC formulations were presented in Fig. 9c. As evidenced from the profile, free Active Ingredient was quickly removed from circulation whereas rCCL-p-HNCs exhib-ited prolonged circulation time. All the pharmacokinetic parameters of CSol and rCCL-p-HNCs were calculated and values are reported in Table 4. Active Ingredient solution revealed mean residence time (MRT) of 2.20 h and $t_{1/2}$ of 1.46 h, whereas rCCL-p-HNCs presented 25-fold and 24-fold increase in MRT and $t_{1/2}$ respectively. Further, 13-fold decrease in clearance was also observed as com-pared with free drug. It also exhibited 13-fold increase in AUC compared with Active Ingredient solution. Superior phar-macokinetic profile of prepared HNCs might be due to the pegylation layer which is responsible for avoidance RES recognition and reduction in liver and spleen uptake allowing HNCs with prolonged blood circulation time [57]. Consequently, the sustained release of Active Ingredient may have contributed to its improved efficacy as observed in the tumour regression studies.

Conclusion

In current investigation, combinatorial delivery of anti-neoplastic drug and siRNA was done to enhance the effectiveness of Active Ingredient in A549 lung cancer cell line. The formulated coloaded nanocarriers were found to have a sustained release profile and imparted stability to the siRNA in presence of serum. These nanocarriers delivered the payload efficiently inside the cells as evident from the transfection efficiency study besides show-ing improvement in loading efficiency of the drug as well as cytotoxicity as compared with the free drug. A higher cell cycle arrest at specific stage was seen with the coloaded formulation compared with the drug solution. Delivery of ABCC3 siRNA complexed HNCs for ABCC3 protein exerted knock-down of expression leading to sensitization of cancer cells to Active Ingredient. A significant reduction in tumour growth along with superior phar-macokinetics profile was observed with the formulation. Thus, this approach has potential for effective management of cancer using genomic approach with improved therapeutic index and could be able to reduce dose dependent toxicity of the Active Ingredient.

Acknowledgements The authors are thankful to Prof. Paola Luciani (Former Professor of Phospholipids in drug delivery at Friedrich schiller university of Jena) for providing laboratory and technical support in completion of current work and Dr Bhavin Vyas (Head, Depart-ment of Pharmacology, Maliba Pharmacy College, Uka Tarsadia University, Bardoli) for providing facilities for animal studies. The authors acknowledge support from Indian institute of technology (IIT), Gandhinagar for AFM studies, Prof Ashish Ganguly of Institute of microbial technology (IMTech), Chandigarh for SAXS studies, Sun Pharmaceutical advanced research centre (SPARC), Vadodara for Cryo-TEM studies.

Funding This work was supported by Department of Science and Tech-nology (DST), Government of India and German academic exchange service (DAAD), a collaborative project between Faculty of Pharmacy, The Maharaja Sayajirao University of Baroda and Friedrich schiller university of Jena, Germany. The contingency grant was provided by University grant commission (UGC), Government of India.

Compliance with ethical standard

Conflict of interest The authors declare that they have no competing interests.

References

1. Torre LA, Siegel RL, Jemal A. Lung cancer statistics. Lung cancer and personalized medicine. Springer; 2016. p. 1–19.
2. Stewart DJ. Lung cancer: prevention, management, and emerging therapies. Springer Science & Business Media; 2010.
3. Saraswathy M, Gong S. Different strategies to overcome multidrug resistance in cancer. Biotechnol Adv. 2013;31(8):1397–407.
4. Szakács G, Paterson JK, Ludwig JA, Booth-Genthe C, Gottesman MM. Targeting multidrug resistance in cancer. Nat Rev Drug Discovery. 2006;5(3):219–34.
5. Chen Ba, Pp Mao J, Cheng FG, Xia Gh, Xu Wl, et al. Reversal of multidrug resistance by magnetic Fe3O4 nanoparticle copolymerizating Active Ingredient and MDR1 shRNA expression vector in leukemia cells. Int J Nanomed. 2010;5:437.
6. Zhao Y, Lu H, Yan A, Yang Y, Meng Q, Sun L, et al. ABCC3 as a marker for multidrug resistance in non-small cell lung cancer. Scientific reports. 2013;3:3120.
7. Creixell M, Peppas NA. Co-delivery of siRNA and therapeutic agents using nanocarriers to overcome cancer resistance. Nano today. 2012;7(4):367–79.
8. Misra A. THERAPEUTIC siRNA : DELIVERYCHALLENGES.
9. Misra A. Challenges in delivery of therapeutic genomics and proteomics. Elsevier; 2010.
10. Gao Z, Zhang L, Sun Y. Nanotechnology applied to overcome tumor drug resistance. J Control Release. 2012;162(1):45–55.
11. Arora S, Rajwade JM, Paknikar KM. Nanotoxicology and in vitro studies: the need of the hour. Toxicol Appl Pharmacol. 2012;258(2):151–65.
12. Blanco E, Shen H, Ferrari M. Nanoparticle rational design implementation for overcoming delivery barriers. Nat Biotechnol. 2015;33:941–51.
13. Jia F, Liu X, Li L, Mallapragada S, Narasimhan B, Wang Q. Multifunctional nanoparticles for targeted delivery of immune activating and cancer therapeutic agents. J Control Release. 2013;172(3):1020–34.
14. Schiffelers RM, Ansari A, Xu J, Zhou Q, Tang Q, Storm G et al. Cancer siRNA therapy by tumor selective delivery with ligand-targeted sterically stabilized nanoparticle. Nucleic acids research. 2004;32(19):e149-e.
15. Saad M, Garbuzenko OB, Minko T. Co-delivery of siRNA and an anticancer drug for treatment of multidrug-resistant cancer. Nanomedicine. 2008;3(6):761–76. https://doi.org/10.2217/17435889.3.6.761.
16. Vhora I, Khatri N, Desai J, Thakkar HP. Caprylate-conjugated Active Ingredient for the development of novel liposomal formulation. AAPS PharmSciTech. 2014;15(4):845–57.
17. Zhao P, Wang H, Yu M, Liao Z, Wang X, Zhang F, et al. Active Ingredient loaded folic acid targeted nanoparticles of mixed lipid-shell and polymer-core: in vitro and in vivo evaluation. Eur J Pharm Biopharm. 2012;81(2):248–56.
18. Mandal B, Bhattacharjee H, Mittal N, Sah H, Balabathula P, Thoma LA, et al. Core–shell-type lipid–polymer hybrid nanoparticles as a drug delivery platform. Nanomed Nanotechnol Biol Med. 2013;9(4):474–91.
19. Troutier A-L, Delair T, Pichot C, Ladavière C. Physicochemical and interfacial investigation of lipid/polymer particle assemblies. Langmuir. 2005;21(4):1305–13.
20. Vhora I, Lalani R, Bhatt P, Patil S, Patel H, Patel V, et al. Colloidally stable small unilamellar stearyl amine lipoplexes for effective bmp-9 gene delivery to stem cells for osteogenic differentiation. AAPS PharmSciTech. 2018;19(8):3550–60.
21. Vhora I, Lalani R, Bhatt P, Patil S, Misra A. Lipid-nucleic acid nanoparticles of novel ionizable lipids for systemic BMP-9 gene delivery to bone-marrow mesenchymal stem cells for osteoinduction. Int J Pharm. 2019;563:324–36.
22. Patil S, Bhatt P, Lalani R, Amrutiya J, Vhora I, Kolte A, et al. Low molecular weight chitosan–Active Ingredient conjugate for siRNA delivery with enhanced stability and transfection efficiency. RSC advances. 2016;6(112):110951–63.
23. Garcia-Diez R, Gollwitzer C, Krumrey M, Varga Z. Size determination of a liposomal drug by small-angle X-ray scattering using continuous contrast variation. Langmuir. 2016;32(3):772–8.
24. Chono S, Li S-D, Conwell CC, Huang L. An efficient and low immunostimulatory nanoparticle formulation for systemic siRNA delivery to the tumor. J Control Release. 2008;131(1):64–9.

25. Patil S, Lalani R, Bhatt P, Vhora I, Patel V, Patel H, et al. Hydroxyethyl substituted linear polyethylenimine for safe and efficient delivery of siRNA therapeutics. RSC advances. 2018;8(62):35461–73.
26. Bhatt P, Lalani R, Vhora I, Patil S, Amrutiya J, Misra A, et al. Liposomes encapsulating native and cyclodextrin enclosed Active Ingredient Enhanced loading efficiency and its pharmacokinetic evalu-ation. Int J Pharm. 2018;536(1):95–107.
27. Bhatt P, Narvekar P, Lalani R, Chougule MB, Pathak Y, Sutariya V. An in vitro assessment of thermo-reversible gel formulation containing Active Ingredient nanoparticles for neovascular age-related macular degeneration. AAPS PharmSciTech. 2019;20(7):281.
28. Saloustros E, Mavroudis D, Georgoulias V. Active Ingredient and Active Ingredient in the treatment of breast cancer. Expert Opin Pharmaco-ther. 2008;9(15):2603–16.
29. Zuidam NJ, Gouw HME, Barenholz Y, Crommelin DJ. Physical (in) stability of liposomes upon chemical hydrolysis: the role of lysophospholipids and fatty acids. Biochimica et Biophysica Acta (BBA)-Biomembranes. 1995;1240(1):101–10.
30. Maecker HT, Trotter J. Flow cytometry controls, instrument setup, and the determination of positivity. Cytometry Part A: the journal of the International Society for Analytical Cytology. 2006;69(9):1037–42.
31. Bepler G, Kusmartseva I, Sharma S, Gautam A, Cantor A, Sharma A, et al. RRM1 modulated in vitro and in vivo efficacy of Active Ingredient and platinum in non-small-cell lung cancer. J Clin Oncol. 2006;24(29):4731–7.
32. Morgan KM, Riedlinger GM, Rosenfeld J, Ganesan S, Pine SR. Patient-derived xenograft models of non-small cell lung cancer and their potential utility in personalized medicine. Frontiers in oncology. 2017;7:2.
33. van ErpLakerveld EAAJ, Mulder H, Luytjes W, Ferwerda G, van Kasteren PB. Pathogenesis of respiratory syncytial virus infection in BALB/c mice differs between intratracheal and intranasal inoculation. Viruses. 2019;11(6):508.
34. Nair AB, Jacob S. A simple practice guide for dose conversion between animals and human. Journal of basic and clinical pharmacy. 2016;7(2):27.
35. Zhao X, Li F, Li Y, Wang H, Ren H, Chen J, et al. Co-delivery of HIF1α siRNA and Active Ingredient via biocompatible lipid-polymer hybrid nanoparticles for effective treatment of pancreatic cancer. Biomaterials. 2015;46:13–25.
36. Bardoliwala D, Patel V, Javia A, Ghosh S, Patel A, Misra A. Nanocarriers in effective pulmonary delivery of siRNA: current approaches and challenges. Therapeutic delivery. 2019;10(5):311–32.
37. Chan JM, Zhang L, Yuet KP, Liao G, Rhee J-W, Langer R, et al. PLGA–lecithin–PEG core–shell nanoparticles for controlled drug delivery. Biomaterials. 2009;30(8):1627–34.
38. Mare R, Paolino D, Celia C, Molinaro R, Fresta M, Cosco D. Post-insertion parameters of PEG-derivatives in phosphocholine-liposomes. Int J Pharm. 2018;552(1–2):414–21.
39. Wang Q, Alshaker H, Böhler T, Srivats S, Chao Y, Cooper C, et al. Core shell lipid-polymer hybrid nanoparticles with combined Active Ingredient and molecular targeted therapy for the treatment of metastatic prostate cancer. Scientific reports. 2017;7(1):1–8.
40. Štarha P, Trávníček Z, Popa I, Dvořák Z. Synthesis, characteriza-tion and in vitro antitumor activity of platinum (II) oxalato com-plexes involving 7-azaindole derivatives as coligands. Molecules. 2014;19(8):10832–44.
41. Khatri N, Rathi M, Baradia D, Misra A. cRGD grafted siRNA nano-constructs for chemosensitization of Active Ingredient hydrochlo-ride in lung cancer treatment. Pharm Res. 2015;32(3):806–18.
42. Rabanel J-M, Hildgen P, Banquy X. Assessment of PEG on polymeric particles surface, a key step in drug carrier translation. J Control Release. 2014;185:71–87.
43. Nakamura K, Yamashita K, Itoh Y, Yoshino K, Nozawa S, Kasukawa H. Comparative studies of polyethylene glycol-modified liposomes prepared using different PEG-modification methods. Biochimica et Biophysica Acta (BBA)-Biomembranes. 2012;1818(11):2801–7.
44. Zhang L, Hu Y, Jiang X, Yang C, Lu W, Yang YH. Camptothecin derivative-loaded poly (caprolactone-co-lactide)-b-PEG-b-poly (caprolactone-co-lactide) nanoparticles and their biodistribution in mice. J Control Release. 2004;96(1):135–48.
45. Li X, Li R, Qian X, Ding Y, Tu Y, Guo R, et al. Superior antitumor efficiency of Active Ingredient-loaded nanoparticles by intratumoral delivery with decreased tumor metabolism rate. Eur J Pharm Biopharm. 2008;70(3):726–34.
46. Płaczek M, Kosela M. Microscopic methods in analysis of submicron phospholipid dispersions. Acta Pharmaceutica. 2016;66(1):1–22.
47. Ruozi B, Belletti D, Tombesi A, Tosi G, Bondioli L, Forni F, et al. AFM, ESEM, TEM, and CLSM in liposomal characterization: a comparative study. Int J Nanomed. 2011;6:557.
48. Ren F, Chen R, Wang Y, Sun Y, Jiang Y, Li G. Active Ingredient-loaded poly (n-butylcyanoacrylate) nanoparticle delivery system to overcome multidrug resistance in ovarian cancer. Pharm Res. 2011;28(4):897–906.
49. Nishiyama N, Okazaki S, Cabral H, Miyamoto M, Kato Y, Sugiyama Y, et al. Novel i-incorporated polymeric micelles can eradicate solid tumors in mice. Can Res. 2003;63(24):8977–83.
50. Gryparis EC, Hatziapostolou M, Papadimitriou E, Avgoustakis K. Anticancer activity of Active Ingredient-loaded PLGA-mPEG nano-particles on LNCaP prostate cancer cells. Eur J Pharm Biopharm. 2007;67(1):1–8.
51. Xu P, Van KirkLi EAS, Murdoch WJ, Ren J, Hussain MD, et al. Highly stable core-surface-crosslinked nanoparticles as Active Ingredient carriers for cancer chemotherapy. Colloids Surf, B. 2006;48(1):50–7.
52. Khatri N, Rathi MN, Baradia D, Trehan S, Misra A. In vivo delivery aspects of miRNA, shRNA and siRNA. Critical Reviews™ in Therapeutic Drug Carrier Systems. 2012;29(6).
53. Qu M-H, Zeng R-F, Fang S, Dai Q-S, Li H-P, Long J-T. Liposome-based co-delivery of siRNA and Active Ingredient for the synergis-tic treatment of lung cancer. Int J Pharm. 2014;474(1–2):112–22.
54. Fröhlich E. The role of surface charge in cellular uptake and cytotoxicity of medical nanoparticles. Int J Nanomed. 2012;7:5577.
55. Prabhakar U, Maeda H, Jain RK, Sevick-Muraca EM, Zamboni W, Farokhzad OC et al. Challenges and key considerations of the enhanced permeability and retention effect for nanomedicine drug delivery in oncology. AACR; 2013.
56. Sadat SM, Jahan ST, Haddadi A. Effects of size and surface charge of polymeric nanoparticles on in vitro and in vivo applications. Journal of Biomaterials and Nanobiotechnology. 2016;7(02):91.
57. Guo S, Huang L. Nanoparticles escaping RES and endosome: challenges for siRNA delivery for cancer therapy. Journal of Nanomaterials. 2011;2011:11.